Journal of Sound and Vibration (2002) 256(4), 605–627
doi:10.1006/jsvi.5011, available online at http://www.idealibrary.com on IDEAL®

# MODEL-ORDER REDUCTION AND PASS-BAND BASED CALCULATIONS FOR DISORDERED PERIODIC STRUCTURES

M. T. Bah, A. Bhaskar and A. J. Keane

*School of Engineering Sciences, University of Southampton, Highfield, Southampton SO17 1BJ, England.*
*E-mail: a.bhaskar@soton.ac.uk*

(*Received* 28 *August* 2001, *and in final form* 22 *January* 2002)

This paper is concerned with the dynamics of disordered periodic structures. The free vibration problem is considered. A method akin to the Rayleigh method is presented. This method is particularly suitable for the study of periodic structures as it exploits the nominal periodicity leading to an approximation that greatly reduces the order of the model. The method is used to calculate the natural frequencies and mode shapes for a pass-band by treating the unknown phases between the nominally identical bays as the generalized co-ordinates of the problem. An illustrative example of a cyclically coupled beam model is presented. In spite of a very large reduction in the computational effort, the results obtained are very accurate both for frequencies and mode shapes even when strong mode localization is observed. To test the performance of the proposed approximation further, a situation where two pass-bands are brought close to each other is considered (a coupled beam model having inherent bending–torsion coupling). The method presented here is general in its formulation and has the potential of being used for more complex geometries.


## 1. INTRODUCTION

Many engineering structures exhibit nearly periodic geometry. They constitute two main classes. First, there are those that possess translational periodicity such as those found in truss beams, multi-span beams, large space structures, etc. In this case, the structural geometry repeats itself as the position is shifted along the direction of periodicity. A structural unit that repeats itself is often referred to as a bay. The second category is that of structures that are rotationally periodic—bladed disc assemblies such as those found in turbo-machinery or, web-like structures with rotational periodicity as found in many domes, spacecrafts, etc., are examples. In the case of rotational periodicity, the geometry of a sector is found to repeat itself at regular angular intervals as one rotates around the centre of symmetry. This paper is concerned with the free vibration behaviour of this latter class of periodic structures. The terms "sector" or "bay" are used synonymously.

Periodic structures possess a characteristic eigenstructure associated with free vibration. They are characterized by unattenuated propagating waves in frequency pass-bands and attenuated standing waves in frequency stop-bands. The free vibration natural frequencies occur in pass-bands with corresponding periodic or extended mode shapes [1].

A rotationally periodic structure that does not have any amount of disorder is often called a tuned system. It is well known that the solution to the problem of tuned systems requires analysis of only one bay or sector. For a tuned system, the modal amplitude of each bay is identical and the inter-bay phase depends on the particular mode in question. When

0022-460X/02/$35.00 

the assembly is mistuned, a particular mode may be "localized". This means that the mode shape is such that the spatial variation of amplitude for different sectors is not uniform and one (or a few) bay(s) may have appreciably large amplitude relative to the rest. The amplitude decays exponentially away from the most-active region (i.e., bay or sector). This phenomenon is known as mode localization. Real structures are seldom perfectly tuned since manufacturing and material variations are inevitable, and variations do occur during service. Therefore, this interesting problem is also a very practical one.

The localization phenomenon was first studied by Anderson [2] in the context of solid-state physics. Crystal lattices are examples of periodic structures and impurities bring in disorder. The difficulty in the context of solid-state physics is that most real problems are not one dimensional. On the other hand many engineering problems show truly one-dimensional periodicity. Hodges [3] was perhaps the first to study Anderson localization in engineering vibration and structural acoustics. Since this seminal work, the problem has attracted the attention of many researchers [4, 5]. For a review of developments on the effects of mistuning on mode localization in periodic structures, see references [6–8]. Perturbation methods [5, 9, 10], wave propagation and transfer matrix methods [7, 11–13] have been extensively used to study disordered periodic systems.

This work is motivated by the need to understand the dynamics of turbine blade assemblies. There are several mathematical idealizations for these structures in the literature. Single-degree-of-freedom models for each blade have been used in references [9, 10]. Afolabi [14] has used a lumped parameter model for the idealization of a blade and a receptance analysis to study bladed disc assemblies. A finite element discretization has been used to represent the individual blades in reference [15]. Various coupled oscillator models of different sophistication have been developed in reference [16] for the modelling of turbomachinery rotors.

Beside these, component mode synthesis methods are also widely used to study coupled component structural systems [17, 18]. These methods consist essentially of a separate determination of the modes of each component followed by a synthesis of the entire system modes. This is convenient when the number of generalized co-ordinates is to be reduced. Modelling the interface between the coupled components of a complex structural system remains difficult. Apart from these methods, the U-transformation technique [19] has been used to analyze nearly cyclic periodic and linear structures and applied to investigate the mode localization phenomena.

For a tuned system, computational simplification results from a known spatial phase relationship among the bays or the sectors in a normal mode, as will be discussed in the next section. However, when each subsystem accounts for a considerable number of degrees of freedom and mistuning is to be included in the analysis, the computational cost is high since the full dynamic problem must be solved. The computational analysis becomes even more expensive when one is interested in the system's sensitivity to mode localization and accurate statistics are needed. The direct calculation for a large number of random realizations affords exact answers but it requires a large number of repeated calculations each of which is expensive. Various statistical or probabilistic approaches have been developed and applied to such structural systems involving parameter uncertainties. A review of this class of problems can be found in reference [6].

An important step forward had been made in reference [20] to tackle the problem of order reduction for the analysis of mistuned blade assemblies. The reduced-order technique introduced by Castanier *et al.* is based on an FE model of a single disc–blade sector followed by component mode synthesis which leads to a considerable order reduction compared to the original FE model. Its principal advantage is the considerable computational saving compared to solving the dynamic response of the entire mistuned

system for a full industrial turbo-machinery rotor FE model with a reduced set of degrees of freedom [21]. This reduced-order modelling was first applied to unshrouded bladed disc assemblies and has been extended to turbomachinery with shrouded blades [22]. The method achieves model-order reduction by representing each sector by fewer degrees of freedom than those in the original problem.

While there are elaborate structural models of sufficient complexity on one hand, and simple models having a few degrees of freedom per bay on the other hand; accurate and inexpensive approximations are desirable when each bay is represented by several degrees of freedom. The present work is inspired by this need. A method that employs a judicious choice of the generalized co-ordinates is presented and this has the effect of reducing the size of the problem dramatically while incorporating all the structural complexity and achieving good accuracy. The effects of the separation between two neighbouring pass-bands on the accuracy of the approximation is also explored.

The paper is laid out as follows. Spatial phase relations for normal modes of tuned periodic systems are discussed in the next section. Based on the discussions in section 2, a method for calculating modal parameters (natural frequencies and mode shapes) for a particular pass-band is presented in section 3. The method is applicable to mistuned systems as well as tuned systems and is based on treating values of the inter-bay phase as the appropriate generalized co-ordinates. It is applied to a specific example of coupled beam model in section 4. Two cases are considered—when bending and torsion are decoupled due to cross-sectional symmetry and when this coupling exists due to asymmetry of the cross-section. Concluding remarks are given in section 5.

## 2. INTER-BAY PHASE RELATIONSHIPS FOR CYCLICALLY PERIODIC STRUCTURES

When a periodic cyclic structure is tuned, the phase angle between two adjacent sectors for each mode is known and by modelling just one sector of the geometry, the behaviour of the whole structure can be determined. The mode shapes of the whole structure can be obtained by using these phases. The inter-bay phase is given by $\alpha = 2\pi(i-1)/p$, $i = 1, \ldots, p$ where $p$ is the number of sectors in the structure and $i$ is the mode number within a pass-band. The mode shapes, for the entire structure passing from one bay to another, are calculated by accounting for this specified phase variation. Note that the term "phase" here refers to the spatial phase variation observed within the deformed shape of a normal mode of the complete structure—it is not the temporal phase during motion. In a normal mode motion, all the material points in the structure will, of course, be in phase or out of phase by definition. The inter-bay phase information for strictly periodic systems is given by the eigenvectors of a circulant matrix of the same size as the number of sectors (i.e., $p$). This matrix is known as the Fourier matrix [23].

In the absence of any coupling, there will be as many degenerate modes as the number of sectors (or bays). These modes have identical natural frequencies associated with them since the Rayleigh quotient of the whole system will be the same for each degenerate mode.

When weak coupling is introduced, the degeneracy breaks down and the Rayleigh quotient of the whole structure is slightly different for each mode shape that originally corresponded to the degenerate set. For example, if the coupling is provided by a light spring, the numerator of the Rayleigh quotient will slightly increase due to the spring contribution—this manifests in a slight increase in all the natural frequencies (*except* the lowest one in each pass-band for which the corresponding mode shape is such that the spring does not compress or stretch). This means that the corresponding natural frequencies

are now slightly different (in fact, increased) for each perturbed mode. The set of these slightly different frequencies is the so-called pass-band that corresponds to what was a single frequency of the order of the number of bays.

The number of pass-bands equals the number of degrees of freedom required to represent the motion of each sector: if for example, in a finite element formulation, one has $q$ number of degrees of freedom, in principle one could calculate natural frequencies for $q$ number of pass-bands. It proves to be convenient to refer to a particular mode for the complete system by referring to the relevant pass-band number and the mode number within this pass-band (the numbering for modes starts with 1 within each pass-band). The generic shape for each sector for a particular pass-band is the same when the system is tuned. For example, if one thinks of each sector being represented by a beam having light coupling springs at the tips (this example will be discussed later in section 4), the mode shape $\tilde{\boldsymbol{\varphi}}^{(1)}$ for all the sectors for all the modes within the *first pass-band* will have no nodes along the spans of the beams; $\tilde{\boldsymbol{\varphi}}^{(2)}$ for all the sectors for the modes within the *second pass-band* will have one node; $\tilde{\boldsymbol{\varphi}}^{(3)}$ for all the sectors for all the modes within the *third pass-band* will have two nodes; and so on.

Using the notation of the direct product (or the Kronecker product), the generalized co-ordinates of the whole system are given by the direct product of the $k$th column $\mathbf{f}^{(k)}$ of the Fourier matrix and the set of generalized co-ordinates of a sector $\tilde{\boldsymbol{\varphi}}^{(i)}$

$$\boldsymbol{\varphi}^{(i,k)} = \mathbf{f}^{(k)} \otimes \tilde{\boldsymbol{\varphi}}^{(i)}, \quad i = 1, \ldots, q \quad k = 1, \ldots, p, \tag{1}$$

where the $l$th component of $\mathbf{f}^{(k)}$ is given by $f_l^{(k)} = \mathrm{e}^{\mathrm{j}2\pi(k-1)(l-1)/p}$, $l = 1, \ldots, p$. The superscript $i$ in the expression $\boldsymbol{\varphi}^{(i,k)}$ refers to the pass-band number, $k$ refers to the mode number within a pass-band; and $l$ in the expression for $f_l^{(k)}$ denotes the sector number. The inter-bay phase for the $k$th mode within a pass-band can be seen to be $2\pi(k-1)/p$. Note that as one goes round the cyclic structure by one cycle, the phase shift is by an amount $2\pi$ as should be expected since the phase of a point with respect to itself must be zero. Note that the total number of degrees of freedom for the whole system is $p$ times that for a sector. Also $\tilde{\boldsymbol{\varphi}}^{(i)}$ can be a spatial function for continuum representation—then $\boldsymbol{\varphi}^{(i,k)}$ is a vector of functions.

While a pass-band consists of a number of slightly perturbed frequencies clustered around the degenerate frequencies, the story of the mode shapes of the mistuned system is more subtle. The overall mode shape for the entire structure may not result in small changes due to slight differences in the individual blades. The well-known phenomenon of mode localization may be observed when one of the sectors has very large amplitude relative to others.

A statistical study of a large population of coupled blade assemblies is of great practical interest. A straightforward but prohibitively expensive approach is to use Monte Carlo simulations and generate a large population of candidate structures (say, $M$) that are nominally identical but slightly different. The computational resources required to carry this out are enormous since an assembly involves a large number of degrees of freedom and the total effort is multiplied by the number of individuals in the population. If $q$ is the number of degrees of freedom per blade; and if $p$ is the number of sectors in the assembly, the total number of degrees of freedom for all the sectors is $N = p \times q$. Generally, $p \ll q$. Therefore, a Monte Carlo simulation amounts to solving a problem of size $N$, $M$ number of times.

The work presented here is motivated by this application. One could use a method such as the assumed modes method with the modes of the tuned system as the basis and work out the frequencies and mode shapes for a mistuned system. In that case, $p$ number of tuned system mode shapes $\boldsymbol{\varphi}_1^{(i)}, \boldsymbol{\varphi}_2^{(i)}, \ldots, \boldsymbol{\varphi}_p^{(i)}$ (of the complete structure) correspond to the $i$th

pass-band of the tuned system and the mode shape of the actual mistuned system is given in the usual way by

$$\hat{\boldsymbol{\varphi}}^{(i)} = \sum_{j=1}^{p} c_j \boldsymbol{\varphi}_j^{(i)}, \tag{2}$$

where $c_j$ are the unknown coefficients. An appropriate variational principle can then resolve the undetermined coefficients—there will be $p$ number of combinations for each set $c_j, j = 1, \ldots, p$.

This will be a satisfactory approach as long as one does not observe localization. When there is a combination of parametric perturbations such that it leads to localization, the approach will fail to predict this since the mode shape (for the combined structure) will be quite different from any one of the tuned system mode shapes and, therefore, a linear combination of these will fail to produce the actual localized mode. In linear algebraic terms, the actual localized mode will have a substantial component in the subspace orthogonal to that spanned by the tuned system modes (that was considered as the basis).

To resolve this, an alternative way of defining the basis is proposed here. This, as will be seen, leads to very substantial saving in computational effort while giving exceptionally accurate "approximate" mode shapes and pass-band natural frequencies.

An assumption of the method developed here is that pass-bands are reasonably well separated. This means that each pass-band is narrow compared to the neighbouring band-gap(s) (or stop-band(s)). This is a reasonable assumption for most practical cases that are weakly coupled. As remarked in the previous paragraph, the overall mode shape for the complete structure changes substantially (from the corresponding tuned system modes) when localization occurs. However, the crucial point is that the *deformed shape of the individual bays does not vary appreciably*. This observation is used profitably in the method proposed here. Moreover, the *shape* of each bay (that may have very different amplitude) is pretty much the same as that corresponding to the shape of a sector for the *tuned* case. Therefore, one can perform calculations for a pass-band by using just one mode shape as the basis (in the spirit of the component modes, the interesting point being that each component is now *identical* for a periodic structure). A most impressive part of the computational economy offered by the proposed method is that $M$ Monte Carlo calculations involve solution of one single sector problem plus $M$ number of Monte Carlo simulations—each of size just $p \times p$!

## 3. CALCULATION OF MODAL QUANTITIES FOR A PASS-BAND

An approximation is now presented for calculating the modal quantities based on energy considerations and the Rayleigh method. The kinetic energy and the potential energy expressions for the complete structure are given by

$$T(t) = \tfrac{1}{2}\,\dot{\mathbf{u}}^{\mathrm{T}}\mathbf{M}\dot{\mathbf{u}}, \qquad V(t) = \tfrac{1}{2}\,\mathbf{u}^{\mathrm{T}}\mathbf{K}\mathbf{u}, \tag{3}$$

where $\mathbf{u}$ is the vector of the generalized co-ordinates of size $N = p \times q$. For synchronous free vibration, the existence of non-trivial motion requires

$$\mathbf{K}\boldsymbol{\varphi} = \lambda\,\mathbf{M}\boldsymbol{\varphi}, \tag{4}$$

which has $N$ solutions for $\lambda$ and $\boldsymbol{\varphi}$. Equation (4) is computationally an expensive step particularly for large systems (i.e., when $N$ is large). It also happens to be an essential step for most response calculations. It is an objective of this paper to present an economical method

that replaces solution of equation (4) by a computationally cheap but reasonably accurate calculation.

It is proposed to represent the deformed shape of the complete structure in the $i$th pass-band by the following vector:

$$\hat{\boldsymbol{\varphi}}^{(i)} = \{a_1\boldsymbol{\psi}^{(i)^{\mathrm{T}}}, a_2\boldsymbol{\psi}^{(i)^{\mathrm{T}}}, \ldots, a_p\boldsymbol{\psi}^{(i)^{\mathrm{T}}}\}^{\mathrm{T}}, \tag{5}$$

where $\boldsymbol{\psi}^{(i)}$ is the $i$th mode shape of a single bay or sector (of course, in the absence of mistuning). Equation (5) asserts that the generalized co-ordinates for the entire structure are approximated by choosing a different scaling for each tuned sector mode shape and stacking these co-ordinates one after another. The scaling factors $a_j$, $j = 1, \ldots, p$ play an important role in the analysis now, because they can be viewed as a new set of generalized co-ordinates.

In other words for each pass-band only one assumed mode is chosen, i.e., one generalized co-ordinate per subsystem. In the notation of the Kronecker product, one can write the approximation of equation (5) as

$$\hat{\boldsymbol{\varphi}}^{(i)} = \mathbf{a} \otimes \boldsymbol{\varphi}^{(i)}, \tag{6}$$

where $\mathbf{a} = \{a_1, a_2, \ldots, a_p\}^{\mathrm{T}}$ is the vector of unknown coefficients $a_j$ yet to be determined.

The assumption of equation (5), (or equivalently equation (6)), amounts to imposing a constraint on the possible deformation since it admits only special deformed shapes for each sector. However, it may be claimed that the most crucial freedom required in the problem is allowed—the amplitudes of the individual bays can be substantially different (and of differing spatial phase)—these are afforded by the free parameters $a_j$. The variational principle "adjusts" these proportions in the best possible manner as guaranteed by the Rayleigh method. It is interesting to compare equation (6) with equation (1). While the phases are given strictly by the "fundamental phase" for a tuned periodic structure as in equation (1); they can be quite different from these values when disorder is present. The approach here is to resolve these unknown phases by the use of an appropriate variational principle. The basic mode shape of an individual bay (it is assumed), remains approximately unchanged if the disorder is small.

The mode shape for a sector or a bay $\boldsymbol{\psi}^{(i)}$ may be an analytical mode shape or a mode shape determined from an appropriate discretization for a sector. In the case of an analytical mode shape, this needs to be treated as a function of spatial variables, else it is a vector of the relevant generalized co-ordinates. In any case, given the deformed shape of the entire structure as in equation (5), the total kinetic energy and the potential energy of the system are quadratic forms in the unknowns $a_j$ and, therefore,

$$T(t) = \tfrac{1}{2}\,\dot{\mathbf{a}}^{\mathrm{T}}\bar{\mathbf{M}}\dot{\mathbf{a}}, \quad V(t) = \tfrac{1}{2}\,\mathbf{a}^{\mathrm{T}}\bar{\mathbf{K}}\mathbf{a}, \tag{7}$$

where $\bar{\mathbf{M}}$ and $\bar{\mathbf{K}}$ are the coefficient matrices that depend on the structural parameters e.g., geometry and material properties. Equation (7) is an approximation for equation (3) since the energy expressions in equation (7) result from "constraining" the system by allowing less freedom than it actually has. Note that the size of $\bar{\mathbf{M}}$ and $\bar{\mathbf{K}}$ in equation (7) is much smaller than $\mathbf{M}$ and $\mathbf{K}$ in the original expressions (3). For this reason we shall call $\bar{\mathbf{M}}$ and $\bar{\mathbf{K}}$ the reduced mass and the reduced stiffness matrices respectively.

For synchronous harmonic motions, $\mathbf{a}(t) = \mathbf{a}\exp(\mathrm{i}\omega t)$, the Rayleigh quotient $R$ is written as

$$R = \frac{\mathbf{a}^{\mathrm{T}}\bar{\mathbf{K}}\mathbf{a}}{\mathbf{a}^{\mathrm{T}}\bar{\mathbf{M}}\mathbf{a}}. \tag{8}$$

Applying the Rayleigh variational principle, the first variation of $R$ must be set to zero, i.e., $\delta R = 0$. This requires that the first derivative of $R$ with respect to each of the yet to be determined unknowns must vanish, i.e.,

$$\frac{\partial R}{\partial a_j} = 0,\ j = 1, \ldots, p. \tag{9}$$

Since the numerator and the denominator of $R$ are quadratic forms, application of conditions (9) results in the following eigenproblems:

$$\bar{\mathbf{K}}\mathbf{a} = \lambda \bar{\mathbf{M}}\mathbf{a}, \tag{10}$$

which is of substantially smaller size than the original eigenproblem (4) since $p \ll pq$. The $p$ number of solutions for $\lambda$ in equation (10) correspond to the square of natural frequencies for the pass-band in question. The entries of the corresponding eigenvectors $\mathbf{a}$ can be substituted into equations (5) or (6) to determine the mode shapes of the complete structure. Typically, $p$ may be of the order of 10–50 whereas $q$ can be anywhere between a thousand to tens of thousands, depending on the complexity of one sector and the level of sophistication used in modelling it. However, note that we must solve one sophisticated problem for a single tuned sector (i.e., a $q \times q$ problem) to determine the fundamental mode shapes. The real gain is in using equation (10) several times in a Monte Carlo simulation since it is an inexpensive step.

An interesting feature of the method proposed here is that one does not need to calculate all the natural frequencies for every pass-band. Calculations can be targeted to pass-bands of particular interest. In practice, the first few pass-bands may be important for low-frequency excitation. Alternatively, for rotating machinery, the frequency bands may be chosen around the narrowband excitation frequencies corresponding to the rotational speed. If the requirement is of calculating all the pass-bands (unlikely for most practical situations), the method still offers computational economy—solving $q$ number of $p \times p$ eigenproblems is substantially cheaper than solving a single eigenproblem of size $pq \times pq$!

## 4. EXAMPLES, RESULTS AND DISCUSSIONS

First consider a coupled beam model of a cyclic structure where stiffness coupling is provided in the plane of the disc. Assuming a doubly symmetric cross-section, torsion and bending deformations are decoupled and, therefore, torsional motions will be kept out of consideration, as they can be determined independently. Under these assumptions and ignoring rotary inertia and shear deformation, the kinetic energy $T(t)$ and the potential energy $V(t)$ of the beam are given by

$$T(t) = \frac{m}{2}\int_0^L \dot{w}^2\,\mathrm{d}x,\ V(t) = \frac{EI}{2}\int_0^L w''^2\,\mathrm{d}x, \tag{11}$$

where the dot represents differentiation with respect to time $t$ and a prime represents differentiation with respect to the spatial co-ordinate $x$ along the beam, the mass per unit length of the beam is $m$, the bending stiffness of the beam is $EI$ and the length is $L$. Using standard finite element methodology, the total energies can be expressed as a sum of energies of the constituent parts (a procedure known as assembly) and a discrete model can be built. The boundary conditions at the root are zero transverse displacement of the beam and a (fairly stiff) rotational spring. This is to simulate the "fir-tree" structure and the flexibility of the mounting of a turbo-machinery-blade fixity. In addition, the rotational

spring provides an opportunity to simulate uncertainty (potentially, appreciably large) at the blade root.

Since the model uses a beam idealization, the parameters that describe the blade geometry and properties are few. Therefore, the results are presented in a non-dimensional form—this also enables one to assess the effect of the relative strength of various parameters on the results of interest. The stiffness matrix and the mass matrix are non-dimensionalized as

$$\bar{\mathbf{K}}^* = \bar{\mathbf{K}}/(EI/L^3), \text{ and } \bar{\mathbf{M}}^* = \bar{\mathbf{M}}/(mL). \tag{12}$$

The tip coupling spring stiffness and the root torsional stiffness are non-dimensionalized as

$$k^* = k_{tip}/(EI/L^3), \text{ and } k^*_{rot} = k_{rot}/(EI/L). \tag{13}$$

Finally, the eigenvalues and the natural frequencies are non-dimensionalized as

$$\lambda^*_l = \lambda_l/(EI/mL^4), \text{ and } \omega^*_l = \omega_l/(\sqrt{EI/mL^4}). \tag{14}$$

### 4.1. AN EXAMPLE OF SIX COUPLED BEAMS

Consider a model built on the basis of the approximations presented in section 3 with six blades. When the non-dimensional coupling stiffness is kept as 0·05, the six degenerate frequencies split into the corresponding pass-bands. The non-dimensional exact eigenvalues for the first pass-band are calculated as 12·3620, 12·5619, 12·5619, 12·9611, 12·9611 and 13·1604. The first of these is expected to be close to the non-dimensional eigenvalue for a single beam. As this value is very close to the theoretical value for a fixed–free cantilever beam (accurate to the third place 12·3596), it indicates that the rotational spring stiffness at the root is high ($k^*_{rot} = 2{\cdot}5 \times 10^6$) and it simulates the fixed boundary condition reasonably well. The value of the disorder is chosen as [0·5%, 2·5%, 7·5%, 4%, 10%, 5%] of $k^*_{rot}$ and is added to the root stiffness. Although these values are reasonably significant, the disorder introduced is small since an appreciable change in an already very high value of stiffness does not change the physical situation very much—the root is practically fixed before and after introducing disorder. This is reflected by the fact that the disorder leaves the degenerate doublets as approximately doublets. The same value of disorder (as a percentage of the baseline value) is felt by the system more dramatically when the inter-bay coupling is reduced. The other alternative is to reduce the baseline value of the root stiffness. Both of these situations will be taken up later.

The width of the pass-band is about 6·5% of the fundamental beam frequency (from 12·3620 to 13·1604) indicating that the coupling is moderate as it spreads the frequencies by an appreciable amount. The non-dimensional eigenvalues as computed on the basis of approximations presented in this paper are calculated as 12·3620, 12·5620, 12·5620, 12·9620, 12·9620 and 13·1620. These values agree extremely well with the corresponding "exact" values as they are all calculated correctly to the fourth place of decimal. Note that the first frequency in each pass-band will be nearly exactly calculated and will be equal to the single beam eigenvalues if the disorder is not too large. This is because the coupling springs are practically inactive for this mode.

The mode shape for the *first mode in the first pass-ban*d is shown in Figure 1. The individual blades are in phase as expected. The solid lines represent the actual deformed shape using an exact analysis. The little dots are the mode shapes obtained from the pass-band-based approximation proposed in this paper. The agreement is indeed extremely satisfactory. This confirms that, in practice, the shape of individual blades is not greatly different than the fixed–free beam modes.

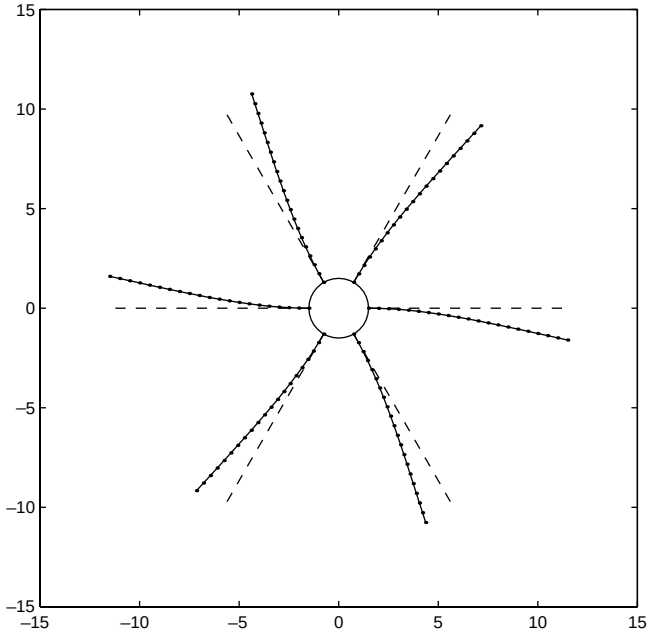


Figure 1. First mode shape in the first pass-band for the strongly coupled six-blade system. The solid lines (—) represent the exact mode shape, the dots ( · ) represent the shape obtained from the proposed approximation and the dashed lines (– – –) represent the undeformed state.

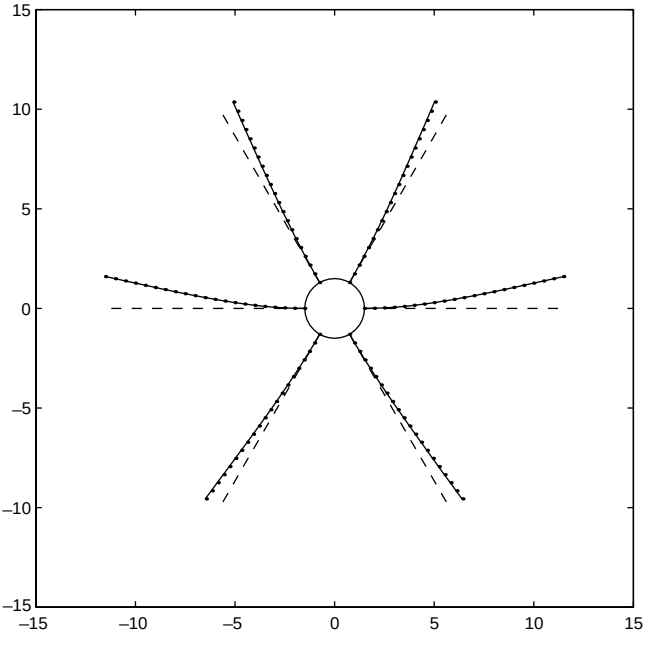


Figure 2. Second mode shape in the first pass-band for the same system as in Figure 1. Same legend as in Figure 1.

The *second mode of the first pass-band* is shown in Figure 2. Note that the beams are not all in phase, in fact, the amplitudes appear in the ratio 1:0·5: — 0·5: — 1: — 0·5:0·5 as expected for this mode. The order of referring to the individual blades is counter-clock wise

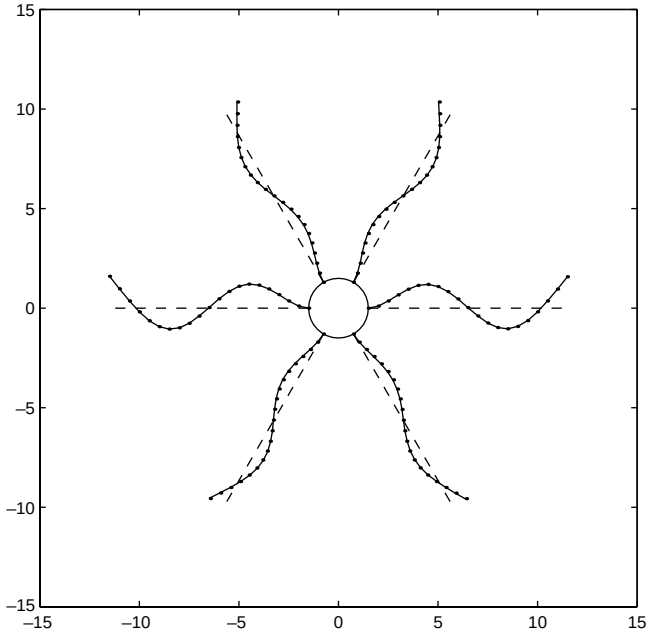


Figure 3. Second mode shape in the third pass-band for the same system as in Figure 1. Same legend as in Figure 1.

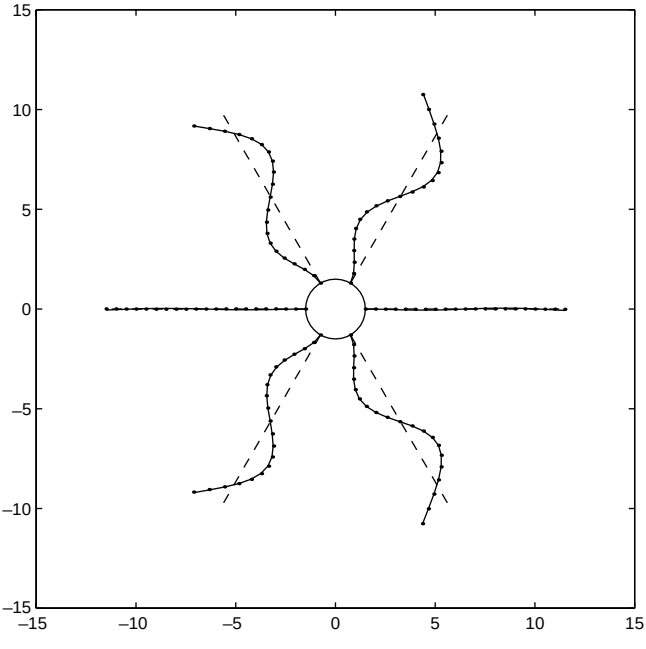


Figure 4. Third mode shape in the third pass-band for the same system as in Figure 1. Same legend as in Figure 1.

starting from the horizontal beam at the "three-o'-clock position" as beam number 1. The approximate mode shapes are quite accurate again; some of the dots do appear to be sliding off the solid line but the agreement is still very good. The same inter-bay phase relationship is maintained for the *second mode of the third pass-band* but the individual beam shapes

resemble the third mode of the fixed–free beam having two nodes each (see Figure 3). The mode shape presented in Figure 4 corresponds to the *third mode of the third pass-band*. The mode shapes in Figures 3 and 4 are very different but they represent a pair of (approximately) degenerate modes.

Keeping the level of disorder as before, the coupling spring is rendered weaker now by setting the value of the non-dimensional coupling stiffness as $5 \times 10^{-5}$. Weak inter-bay coupling is not an unrealistic situation from practical standpoint—aerodynamic coupling can be very weak. As expected, the non-uniformity in amplitude of the individual blades starts showing up now. The first mode of the second pass-band is shown in Figure 5. Note that second blade has larger amplitude than the rest. The width of the pass-band is very small—the six non-dimensional eigenvalues span the range 12·3620–12·3628. These values are again recovered accurate to the fourth decimal place by the use of the approximation presented in this paper. This is expected since the coupling is light. It is interesting to note that the approximate and the exact mode shapes are almost identical and that it confirms that, despite having different amplitudes for each arm of the structure, they all have the same shape since the dots are generated by scaling the fixed–free cantilever modes in the ratio $a_j$ dictated by the Rayleigh quotient minimization.

When the coupling stiffness is progressively increased, the accuracy in calculations using the approximation of equation (5) is expected to deteriorate. For various values of the non-dimensional coupling stiffness in the range 0·1–3·0 the percentage error in calculation of the eigenvalues (defined as the magnitude of error as a fraction of the exact values) is plotted in Figure 6 for the first pass-band. The first mode is calculated exactly and the corresponding error is thus zero. The doublet of the second and the third modes is shown using a solid line. The calculations are accurate within 2%. For the doublet of the fourth and the fifth modes these errors are within 7% (dots on solid line) and for the sixth mode it is within 10% (dashed line). Recalling the non-dimensionalization, $k^* = 3$ corresponds to the

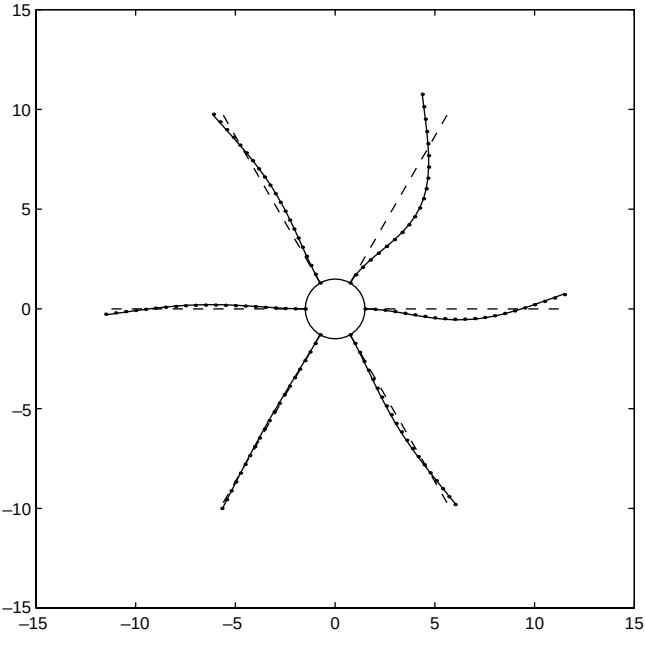


Figure 5. First mode shape in the second pass-band for the weakly coupled six-blade system. Same legend as in Figure 1.

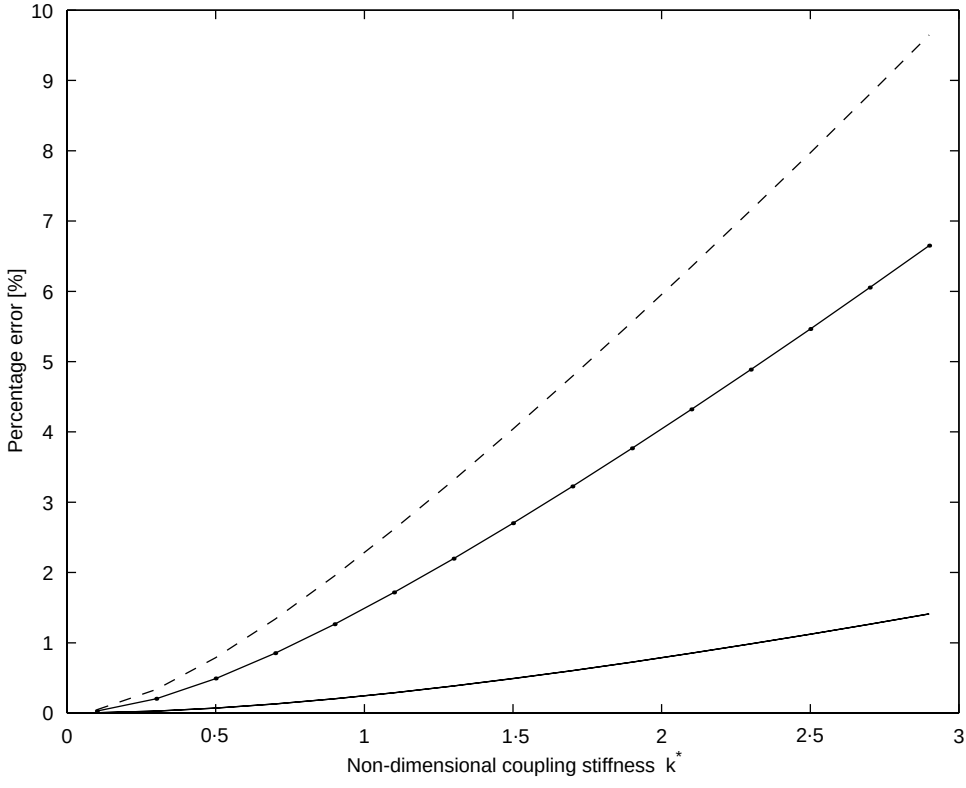


Figure 6. The percentage error in the calculation of the eigenvalues (approximation) in the first pass-band of the coupled six-blade system is plotted as a function of the coupling stiffness between the blades. The solid line (—) corresponds to the doublet of the second and the third modes. The dots (·) on the solid line correspond to the doublet of the fourth and the fifth modes. The dashed line (– – –) corresponds to the sixth mode.

coupling stiffness being equal to the stiffness of a cantilever beam as felt at the tip, since the tip deflection under a load $F$ is given by $(FL^3/3EI)$. In the light of this, the result indeed is quite satisfactory since this should be regarded as a case of very strong coupling. For coupling stiffness equal to 1/10th of the value of beam-tip stiffness, the worst cases of error are well below half-a-per cent. These error values are for eigenvalues—for frequencies the worst errors corresponding to Figure 6 (when the beam-tip stiffness is equal to the coupling stiffness) will be only about 5% since frequencies are square roots of the corresponding eigenvalues. When the coupling stiffness is about 1/10th of the beam-tip static stiffness, the worst errors in frequency are thus well below a quarter of a per cent.

For moderately strong coupling, the width of the pass-band is moderately large. When the value of the non-dimensional coupling stiffness was set to 1 and the disorder set to zero, the exact non-dimensional eigenvalues are calculated as 12·3620, 16·3221, 16·3221, 24·0054, 24·0054 and 27·7300. The corresponding values as computed by the use of approximation (5) are 12·3620, 16·3619, 16·3619, 24·3619, 24·3619 and 28·3618. The width of the pass-band is about 125% of the first eigenvalue in the pass-band. This indicates that the inter-bay coupling is reasonably large. Despite this, the error in computing the last eigenvalue in the pass-band is only 2·28%—a remarkable level of accuracy. This error is due to the fact that the approximation assumes that the shape of the individual beams within a pass-band corresponds to the fixed–free single beam shape. In practice, the tip spring will alter this shape.

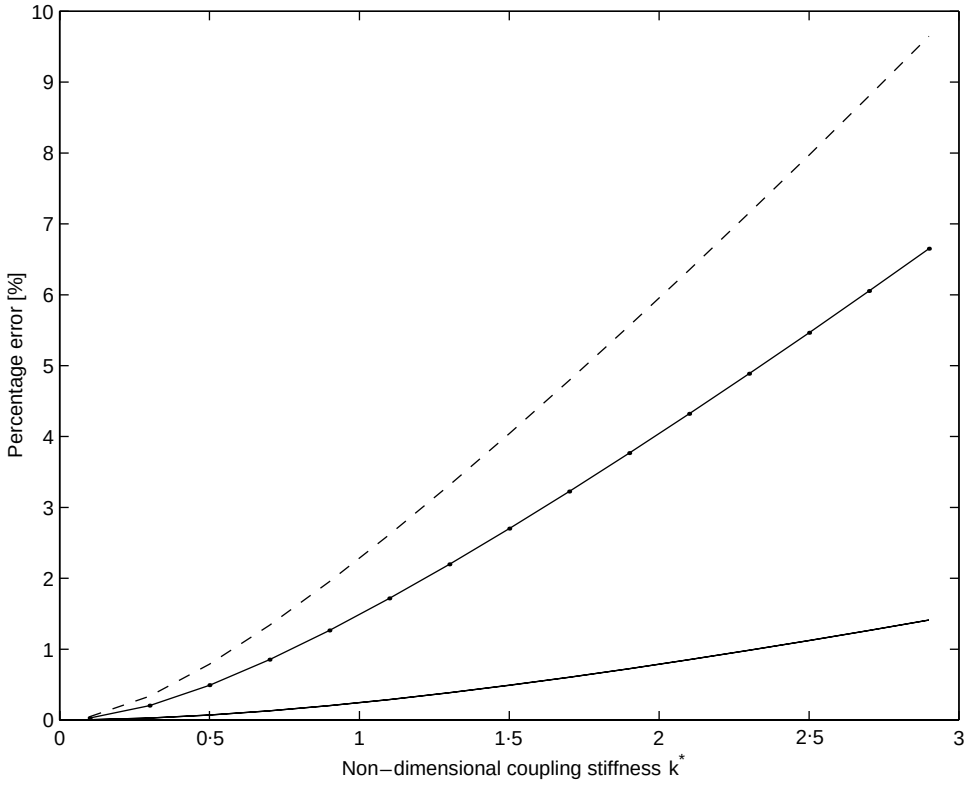


Figure 7. The percentage error in the calculation of the eigenvalues (approximation) in the *second* pass-band of the coupled six-blade system is plotted versus the coupling stiffness between the blades. Same legend as in Figure 6.

The increase in error with mode number within a pass-band is explained by the fact that the lower modes see less relative energy storage within the coupling spring. Therefore, the shapes of individual beams resemble those of the fixed–free beam (the shape chosen to form the basis) in most cases. For the first mode in a pass-band, all the tips are in phase resulting in no energy storage in the coupling and, therefore, the individual beam shapes are exactly the same as a fixed–free beam. For the last mode in a pass-band, all the tips are out of phase giving maximum effectiveness of the coupling springs—this tends to change the shape of the normal mode. For intermediate modes, some of the beams have their tips with ineffective (or less effective) tip springs and others have more effective springs leading to shapes of individual beams ranging from being close to a fixed–free beam to being close to a fixed–sprung beam.

Errors for the second pass-band are shown in Figure 7. The errors are seen to be substantially less than the corresponding values for the first pass-band as shown in Figure 6. The reason is that the coupling strength is effectively smaller for progressively higher pass-bands. The reason for this diminished effective coupling with increasing pass-band number will be explained shortly.

### 4.2. SPATIAL DECAY OF AMPLITUDE FOR A LOCALIZED MODE

To study the bay-wise variation in amplitude of a localized mode, the coupled beam model of a 20-bladed system is presented next. While the six-bladed model was useful in

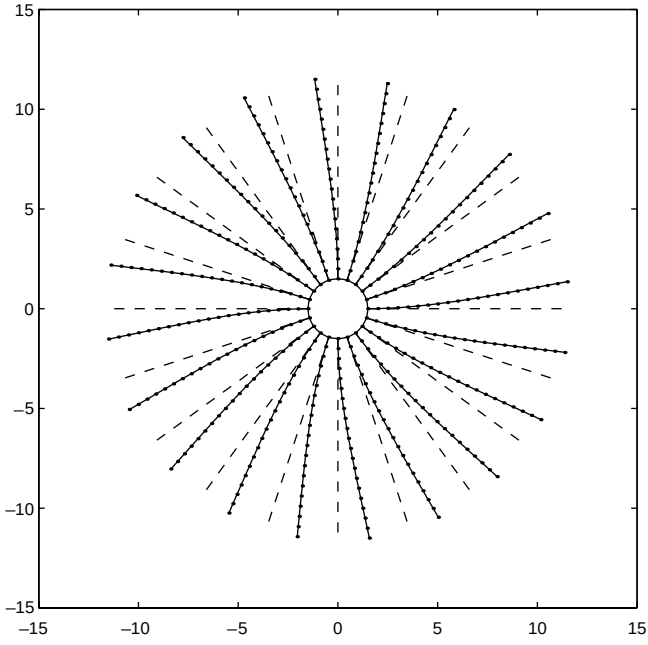


Figure 8. First mode shape in the first pass-band of the coupled 20-blade system. The solid lines (—) represent the exact mode shape, the dots (·) represent the shape obtained from the proposed approximation and the dashed lines (– – –) represent the undeformed state.

understanding different phase relations within a pass-band, a larger number of bays is required for a mode shape to resolve the decay of amplitude away from a high-amplitude bay. The range of disorder studied varies from 0·5 to 5·0% of the baseline value of the root stiffness. The first mode of the first pass-band is nearly unchanged due to the disorder and is shown in Figure 8. For the same disorder, the first mode of the second pass-band is shown in Figure 9 and the first mode of the third pass-band is shown in Figure 10.

Note the progressively increasing localization behaviour with the pass-band number. This is because *for the same level of disorder at the root, the tip coupling is stronger for low pass-band numbers and weaker for high pass-band numbers* as previously remarked. The reason is the greater potential energy stored in the beam (relative to the potential energy of the coupling springs) in the case of modes with high pass-band number: the mode shapes have higher number of nodes now for each beam ensuring that the curve changes its sign about the non-deformed state rapidly meaning that the curvatures are large, hence a larger contribution to the total strain energy since the strain energy density for beams is proportional to the local curvature of the beam (see equation (11)). The kinetic energy expressions do not have terms that couple the adjacent beams. Therefore, coupling becomes progressively weaker as we go higher up the pass-band number in the modal series due to its progressively diminished contribution to the total potential energy. Because of the relatively weaker inter-bay coupling for modes in the higher pass-bands, they are likely to localize more. This explains the difference in the localization behaviour in Figures 8–10.

The increase in amplitude over successive bays for the three modes in Figures 8–10 is presented on a logarithmic scale in Figure 11. Amplitudes for six blades (covering five bays) are plotted such that the right-most blade corresponds to the largest amplitude blade. As predicted by the theory of Anderson localization, these amplitudes show an exponential spatial variation. On a logarithmic plot they are approximately straight lines. For the

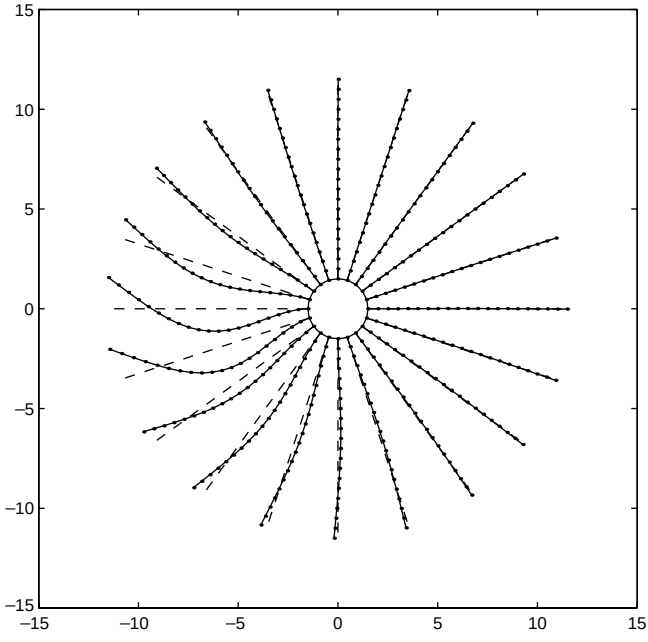


Figure 9. First mode shape in the second pass-band of the coupled 20-blade system. Mistuning and coupling stiffness are the same as in Figure 8. Note the increased localization behaviour as compared to that in Figure 8. Same legend as in Figure 8.

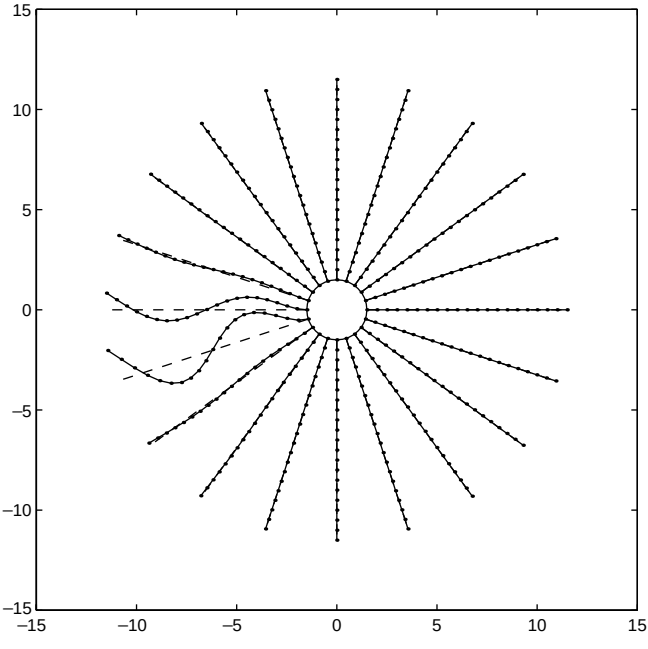


Figure 10. Localization of the first mode shape in the third pass-band of the coupled 20-blade system. Mistuning and coupling stiffness are the same as in Figure 8. Note the stronger localization behaviour as compared to Figures 8 and 9. Same legend as in Figure 8.

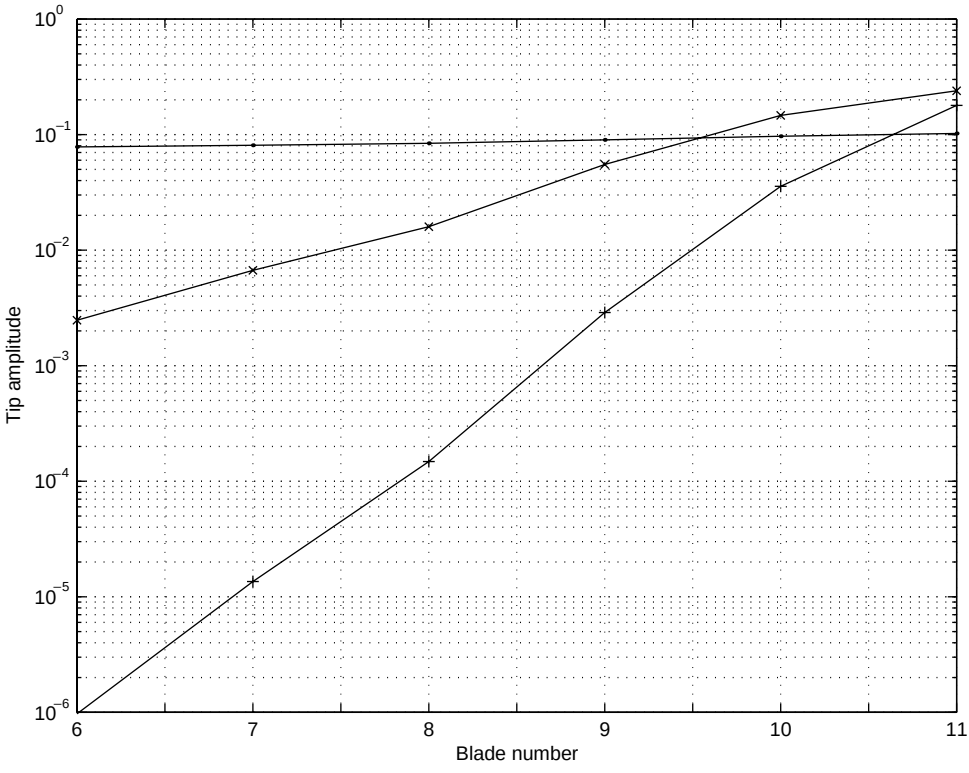


Figure 11. The increase in amplitude over successive bays for the three modes shown in Figures 8–10 is presented on a logarithmic scale. They are plotted as a function of the bay number. The dots ( · ), crosses ( × ) and pluses ( + ) represent the modes in Figures 8, 9 and 10 respectively.

second and the third pass-bands, the slopes are approximately equal to 8·2 and 21 dB/bay respectively. The same number for the first pass-band is less than half dB/bay indicating that it is a nearly extended mode. These Figures correspond to a decrease in amplitude away from a localized blade at a rate of less than 6% reduction per bay in the first pass-band, about 39% per bay for the second pass-band and over one order of magnitude per bay for the third pass-band.

### 4.3. THE EFFECT OF SEPARATION BETWEEN PASS-BANDS ON THE APPROXIMATION

When the neighbouring pass-bands are well separated, the approximation proposed in this paper is likely to work well. This is because each pass-band will have an associated deformed shape for each bay which needs different scaling for different bays—the scale factors, we hope, will be resolved successfully by the variational principle. When two pass-bands come close to each other, the representative shape of the neighbouring pass-band may significantly affect the deformed shape in a normal mode. This may be particularly true for modes at the edges of a pass-band.

To explore the performance of the proposed approximation in this situation, a model of cyclically connected beams that possess torsional degrees of freedom is now considered. The cross-section of each beam is assumed to have a single plane of symmetry that is perpendicular to the plane of the disc. In this case, the bending vibration out of the plane of

the disc is decoupled from the in-plane bending and torsion. The bending motion in the plane of the disc, however, is coupled to the torsional motion. This is the well-known case of "double-coupling" for bending and torsion (see reference [24]). It can be shown that bending–torsion coupling exists when the centroid of the cross-section and the shear centre do not coincide.

Ignoring warping of the cross-section, the potential energy terms are modified by adding a contribution from the twist deformation $\theta$. The kinetic energy expression is given by

$$T(t) = \frac{\rho A}{2}\int_0^L (\dot{v} - \dot{\theta}C_z)^2\,\mathrm{d}x + \frac{\rho I_p}{2}\int_0^L \dot{\theta}^2\,\mathrm{d}x, \tag{15}$$

where $\rho$ is the density, $A$ is the cross-sectional area, $C_z$ is the distance between the centroid and the shear centre, $I_p$ is the second moment of area about the shear centre of the cross-section. This can be expanded as a sum of three terms—one involving the squares of transverse velocity, one involving the square of the rotational velocity and one involving the product of the transverse and rotational velocities

$$T(t) = T_{bending} + \frac{\rho I_0}{2}\int_0^L \dot{\theta}^2\,\mathrm{d}x - C_z\rho A\int_0^L \dot{v}\dot{\theta}\,\mathrm{d}x, \tag{16}$$

where $T_{bending}$ accounts for the kinetic energy term proportional to $\dot{v}^2$ and $I_0$ is the second moment of area about the centroid. It is the third term that leads to bending–torsion coupling. A finite element implementation was achieved by allowing a torsional degree of freedom at each node of the finite element model discussed in the previous example. Disorder was attributed to the root rotational spring as before. The potential energy expression is now modified to

$$V(t) = V_{bending} + \frac{GC}{2}\int_0^L \theta'^2\,\mathrm{d}x, \tag{17}$$

where $G$ is the shear modulus, $C$ is the torsional constant of the cross section and $V_{bending}$ accounts for the potential energy term proportional to $v'^2$. The following two non-dimensional parameters

$$\alpha = I_0/(AC_z^2),\ \beta = GC\,L^2/(EI\,C_z^2), \tag{18}$$

will be used to present the results in this section.

The six-bay model will be considered here—the rotational stiffness of the spring at the root is reduced to $k^*_{rot} = 2{\cdot}5 \times 10^4$ to enhance the effect of disorder. The level of disorder is kept as [0·25%, 0·125%, 0·375%, 0·2%, 0·5%, 0·25%] of the baseline value of the root stiffness. The mode shape for a typical localized mode (first mode of the fifth pass-band) is presented in Figures 12 and 13. The in-plane bending displacements are presented in Figure 12. The solid lines represent the exact mode shape and the dots represent the corresponding bending displacements as calculated from the approximation. The torsional rotation is presented for the same mode in Figure 13. The twist and bending displacements result from a single eigenvector—the two have been shown here with independent normalization for visual clarity. Again, the agreement for the twist is remarkable. Note that the slope of each curve (in Figure 12) is approximately zero at the root as would be expected for a clamped end of a beam. This slope will be exactly equal to zero if the rotational stiffness at the root approaches infinity. The curves for the twist in Figure 13, however, do not show a zero slope at each root as expected. This is because the only geometrical boundary condition for this displacement field is no-twist at the root. The correct localization behaviour is

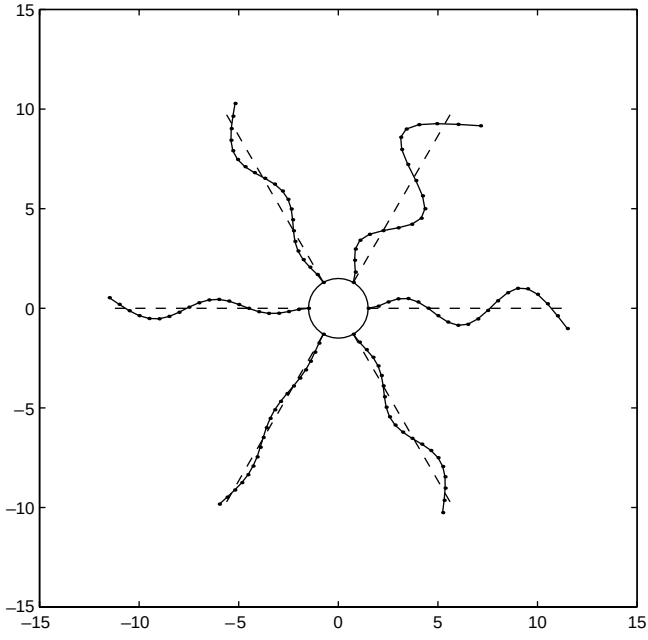


Figure 12. Localization behaviour of the first mode in the fifth pass-band of the coupled 6-blade system having inherent bending–torsion coupling. The *in-plane bending* displacements are plotted against the spatial co-ordinate along the blade. The solid lines ( — ) represent the actual mode shape, the dots ( · ) represent the shape obtained from the proposed approximation and the dashed lines (– – –) represent the undeformed shape.

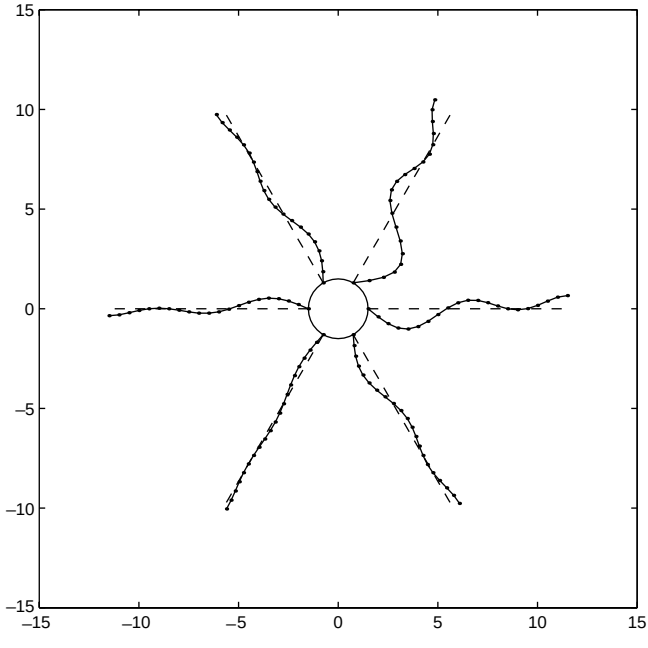


Figure 13. Localization behaviour of the same first mode shown in Figure 12 and for the same system. The *torsional displacements* are plotted here against the spatial co-ordinate along the blade. Same legend as in Figure 12.

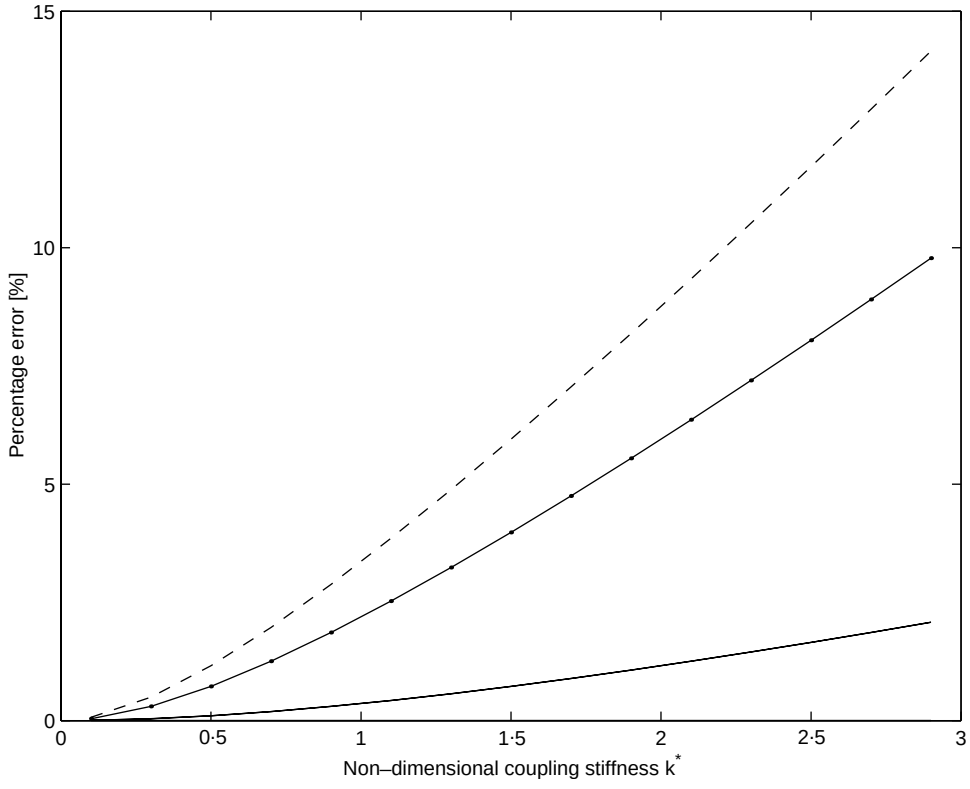


Figure 14. The percentage error in the calculation of the eigenvalues (approximation) in the first pass-band of the coupled 6-blade system having inherent bending-torsion coupling is plotted versus the coupling stiffness between the blades. The solid line (—) corresponds to the second and the third modes. The dots (·) on the solid line correspond to the fourth and the fifth modes. The dashed line (– – –) corresponds to the sixth mode.

predicted by the approximation—one of the concerns with the performance of the proposed method. It is interesting to note that the *actual* deformed shape (obtained from exact calculations and shown using solid lines) for each beam is the same (with different scaling) both for bending as well as the twist co-ordinate: an assumption on which the proposed approximation is based.

Since the mode shapes for the complete structure as obtained from the variational principle resembles the corresponding exact mode shape so well, due to the Rayleigh stationarity principle, the corresponding eigenvalues (or the natural frequencies) agree with the exact ones even better.

The bandwidth of the pass-band is narrow for the case of $\alpha = 20$ and $k^* = 0{\cdot}005$ since the inter-blade coupling is very weak. This was deliberately done in order to test the performance of the proposed method for a mode that may localize (and this happens when the inter-bay coupling is weak). When the coupling stiffness is increased, the percentage errors increase and this dependence is presented for the first pass-band (the worst case situation) in Figure 14. These may be compared with Figure 6 that corresponds to the case without bending–torsion coupling. It is noted that this coupling worsens the performance of the approximation slightly—from the worst error being about 10% in eigenvalue to about 15% (i.e., from being about 5% in frequency to about 7·5%).

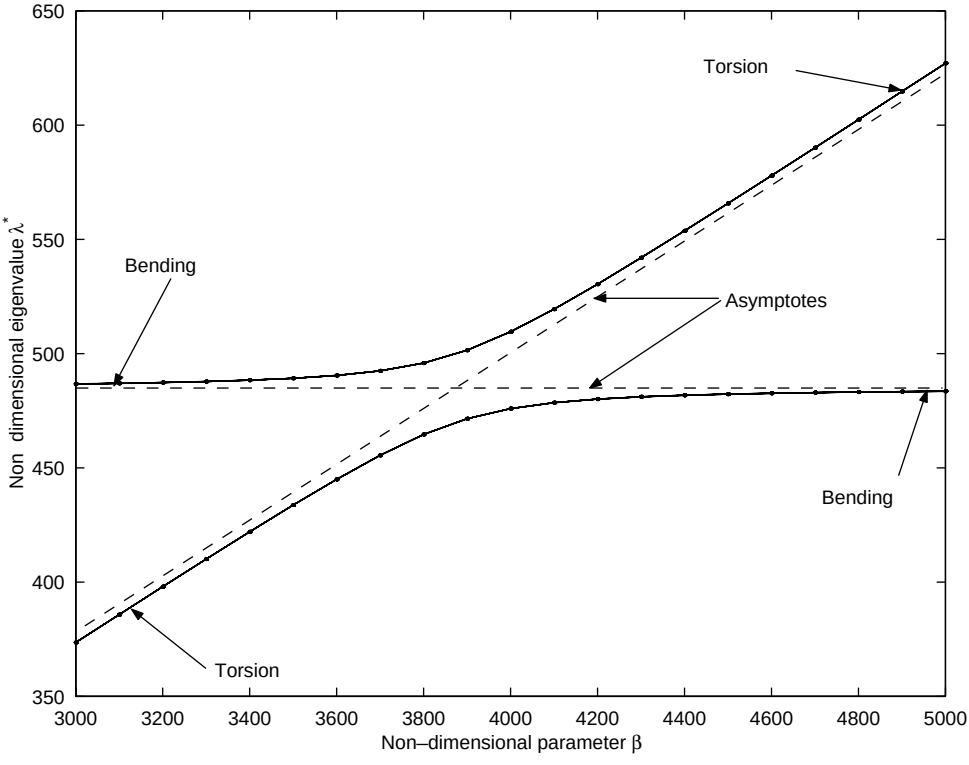


Figure 15. The second and third pass-bands of the weakly coupled 6-blade system are plotted versus the non-dimensional parameter $\beta$ that defines the distance between them. Inter-blade coupling is weak: $k^* = 0{\cdot}005$. The solid lines (—) represent the exact eigenvalues and the dots ($\cdot$) represent the eigenvalues obtained from the proposed approximation.

With the intention of bringing two pass-bands close to each other and to test the performance of the proposed approximation, the value of the non-dimensional parameter $\beta$ was varied while keeping the value of the non-dimensional parameter $\alpha$ constant. If the bending and the torsional modes did not interact via coupling, the uncoupled bending mode will remain unchanged due to a change in $\beta$. The eigenvalue for the torsional mode, on the other hand, will increase linearly with an increase in $\beta$ according to equation (17). These two hypothetical lines will cross at $(\pi^2/4)(\beta/\alpha) = 485{\cdot}48$ (the value of the second non-dimensional eigenvalue for a fixed–free beam). For $\alpha = 20$, the value of $\beta$ to achieve this is 3931·2. In this way, one hopes to see the torsional frequencies being embedded inside a pass-band that corresponds to a bending mode.

The second and third pass-bands are shown in Figure 15. On the left end, the upper branch corresponds to a predominantly bending behaviour and the lower branch represents a predominantly torsional behaviour. On the right end, the order is interchanged—the linearly increasing upper curve represents torsional behaviour and the near constant lower curve represents bending behaviour. This is a classic case of a pair of modes veering against each other. Since the coupling is very weak, the pass-bands are narrow and when overlaid, they are indistinguishable from a pair of veering lines. Note that the eigenvalues are quite satisfactorily reproduced by the approximation—this is true even for the regions of close approach of the two branches of the curves where there is no dominant torsional or bending

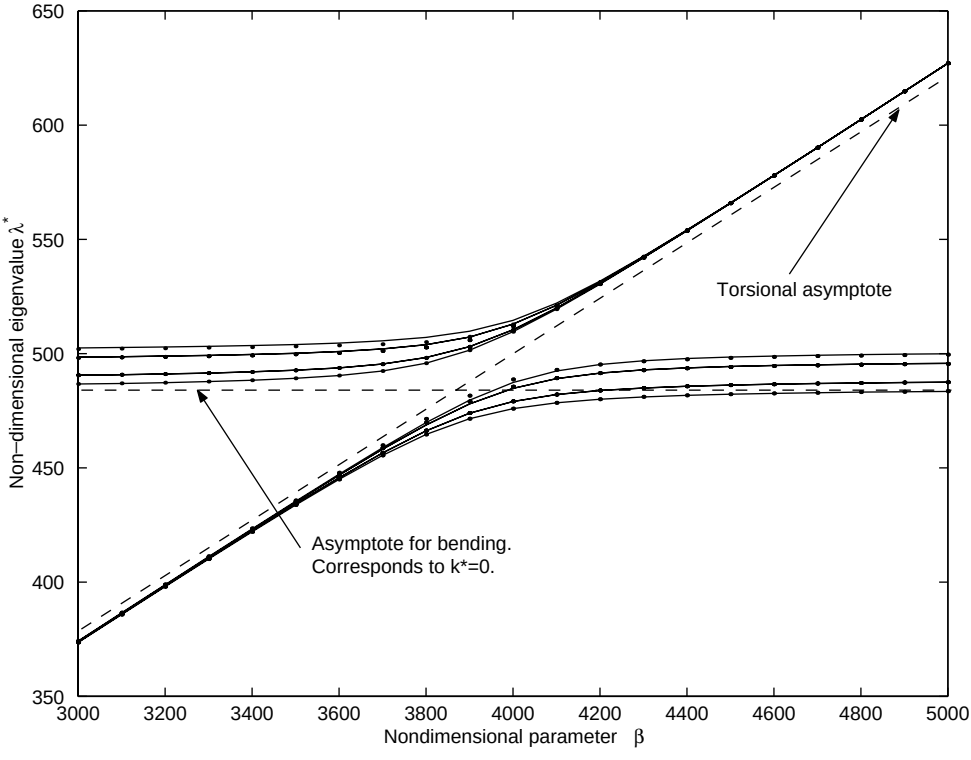


Figure 16. The second and third pass-bands of the coupled 6-blade system are again plotted against $\beta$. Inter-blade coupling is moderately strong and is increased to $k^* = 1{\cdot}0$. The horizontal dashed line corresponds to the asymptote when the inter-blade coupling is ineffective. Same legend as in Figure 15.

behaviour and the modes are of truly mixed character. The reason for the success of the approximation lies in the fact that the single beam modes chosen for the approximation of equation (5) or (6) contains both torsional and bending information from the appropriate eigenvectors of the single beam coupled bending–torsion problem; and this shape does not change much even under the conditions of the two mode types coming close to each other.

When the inter-bay coupling is increased to $k^* = 1{\cdot}0$, the pass-bands widen. The second and third pass-bands are shown as a function of the non-dimensional parameter $\beta$ in Figure 16. The solid lines in each case represent the exact calculations and the dots are the corresponding values as calculated by the use of the approximation. The two pass-bands are seen to veer against each other as two groups of modes. The roughly constant groups of four lines (representing six modes that include two doublets) at the two ends represent the bending behaviour whereas the linearly increasing groups of modes that become narrower and narrower at the ends correspond to the torsional motion. Although the two groups do not ever cross each other, at the centre range of $\beta$ values, the two pass-bands come quite close to each other. As can be seen from Figure 16, the error (although small) is largest in this region. The disagreement between the solid lines (exact calculations) and the dashed lines with dots on them (the approximation) is maximum for the sixth mode for each group around $\beta = 3900$ (which is close to the expected value of $3931{\cdot}2$ when $\alpha = 20$): it is less than $0{\cdot}5\%$ at worst.

The horizontal dashed line corresponds to the asymptotic bending behaviour when the inter-blade coupling is ineffective. This happens for the modes with lowest natural frequency in each pass-band. For other modes, the bending asymptotes are still horizontal but the levels are shifted to higher values—these have been omitted from Figure 16 for clarity.

## 5. CONCLUSIONS

A method of calculating the natural frequencies and mode shapes of a cyclically periodic structure has been presented. The method leads to substantial computational saving by an appropriate choice of generalized co-ordinates. This is achieved by using the component modes for a sector as a basis and by calculating modal quantities for a pass-band at a time. This has the advantage of affording results for a specific pass-band of interest and at a substantially reduced computational expense—the modal quantities for a pass-band are obtained from an eigenproblem of the same size as the number of sectors. For periodic structures having a large number of degrees of freedom for each sector, this strategy offers substantial computational economy; particularly, if one intends to carry out calculations for a large number of cases that are nominally identical, e.g., when one is carrying out Monte Carlo simulations for a large population of samples to gain statistical information.

The proposed method has been applied to a coupled beam model of a bladed disc assembly. The accuracy achieved by the use of the proposed method is remarkable in most cases for various combinations of disorder and coupling. This indicates that the formulation of the model-order reduction allows for all the important degrees of freedom in the problem. In view of the assumptions in the proposed method, this means that the scaling of amplitude for each sector is perhaps the most important degree of freedom and the deviations of the actual deformed shapes of each sector from the assumed ones are negligible. Treating scaling for spatial amplitude as an appropriate degree of freedom results in a successful prediction of mode shapes too, which is crucial for a good understanding of localization behaviour. When applied to an example having each sector represented by beams that possess coupled twist degrees of freedom in addition to bending, the method had been found to be robust in terms of its performance. When two pass-bands (say, one corresponding primarily to bending and one primarily to torsion) are brought close to each other, the two groups of modes veer against each other. This behaviour is fairly accurately captured by the proposed approximation.

## ACKNOWLEDGMENTS

This work was supported by the University Technology Partnership for Design—a partnership between Rolls Royce Plc., BAE Systems and the Universities of Southampton, Cambridge and Sheffield.

## REFERENCES

1. D. J. MEAD 1975 *Journal of Sound and Vibration* **40**, 1–18. Wave propagation and natural modes in periodic systems, I: mono coupled systems.
2. P. W. ANDERSON 1958 *Physical Review* **109**, 1492–1505. Absence of diffusion in certain random lattices.
3. C. H. HODGES 1982 *Journal of Sound and Vibration* **82**, 441–424. Confinement of vibration by structural irregularity.

4. C. H. HODGES and J. WOODHOUSE 1983 *Journal of Acoustical Society of America* **74**, 894–905. Vibration isolation from irregularity in a nearly periodic structure: theory and measurements.
5. C. PIERRE and E. H. DOWELL 1987 *Journal of Sound and Vibration* **114**, 549–564. Localization of vibration by structural irregularity.
6. R. A. IBRAHIM 1987 *Applied Mechanics Reviews* **40**, 309–328. Structural dynamics with parameter uncertainties.
7. C. PIERRE, M. P. CASTANIER and W. J. CHEN 1996 *Applied Mechanics Reviews* **49**, 65–86. Wave localization in multi-coupled periodic structures: application to truss beams.
8. Y. K. LIN 1996 *Applied Mechanics Reviews* **49**, 57–64. Dynamics of disordered periodic structures.
9. S.-T. WEI and C. PIERRE 1988 *Journal of Vibration, Acoustics, Stress, and Reliability in Design* **110**, 429–438. Localization phenomena in mistuned assemblies with cyclic symmetry Part I: free vibrations.
10. G. S. HAPPAWANA, O. D. I. NWOKAH, A. K. BAJAJ and M. AZENE 1998 *Journal of Sound and Vibration* **211**, 761–789. Free and forced response of mistuned linear cyclic systems: a singular perturbation approach.
11. T. T. SOONG and J. L. BOGDANOFF 1963 *International Journal of Mechanical Sciences* **5**, 237–265. On the natural frequencies of a disorder chain of $N$ degrees of freedom.
12. S. T. ARIARATNAM and W.-C. XIE 1995 *Journal of Sound and Vibration* **181**, 7–22. Wave localization in randomly disordered nearly periodic long continuous beam.
13. C. PIERRE 1990 *Journal of Sound and Vibration* **139**, 111–132. Weak and strong vibration localization in disordered structures: a statistical investigation.
14. D. AFOLABI 1988 *Journal of Sound and Vibration* **122**, 535–545. A note on the rogue failure of turbine blades.
15. S.-H. HSIEH and J. F. ABEL 1995 *Journal of Sound and Vibration* **182**, 91–107. Comparison of two finite element approaches for analysis of rotating bladed-disk assemblies.
16. G. OTTARSON 1994 *Ph.D. Dissertation, University of Michigan.* Dynamic modeling and vibration analysis of mistuned bladed disks.
17. W. C. HURTY 1965 *American Institute of Aeronautics and Astronautics* **3**, 678–685. Dynamic analysis of structural systems using component modes.
18. R. R. CRAIG and M. C. C. BAMPTON 1968 *American Institute of Aeronautics and Astronautics* **6**, 1313–1319. Coupling of substructures for dynamic analyses.
19. H. C. CHAN and C. W. CAI 1998 *Journal of Sound and Vibration* **213**, 89–106. Dynamics of nearly periodic structures.
20. M. P. CASTANIER, G. S. OTTARSON and C. PIERRE 1997 *American Society of Mechanical Engineers Journal of Vibrations and Acoustics* **119**, 439–447. A reduced-order modeling technique for mistuned bladed discs.
21. M. KRUSE and C. PIERRE 1996 *American Institute of Aeronautics and Astronautics* **27**, 227–241. Dynamic response of an industrial turbomachinery rotor.
22. R. BLADH, M. P. CASTANIER and C. PIERRE 1999 *American Society of Mechanical Engineers Journal of Engineering for Gas Turbines and Power* **119**, 515–522. Reduced order modeling and vibration analysis of mistuned bladed disk assemblies with shrouds.
23. P. J. DAVIS 1979 *Circulant Matrices*, New York: Wiley-Interscience.
24. J. M. GERE and Y. K. LIN 1958 *Journal of Applied Mechanics* **80**, 373–378. Coupled vibrations of thin-walled beams of open cross section.